Clouds and the Earth's Radiant Energy System (CERES)

Algorithm Theoretical Basis Document

Estimate of Shortwave Surface Radiation Budget From CERES

(Subsystem 4.6.1)

Zhanqing Li[1]
David P. Kratz[2]

[1]Canada Centre for Remote Sensing, 588 Booth Street, Ottawa, Ontario, Canada K1A0Y7
[2]Atmospheric Sciences Division, NASA Langley Research Center, Hampton, Virginia 23681-0001

June 2, 1997

CERES Top Level Data Flow Diagram

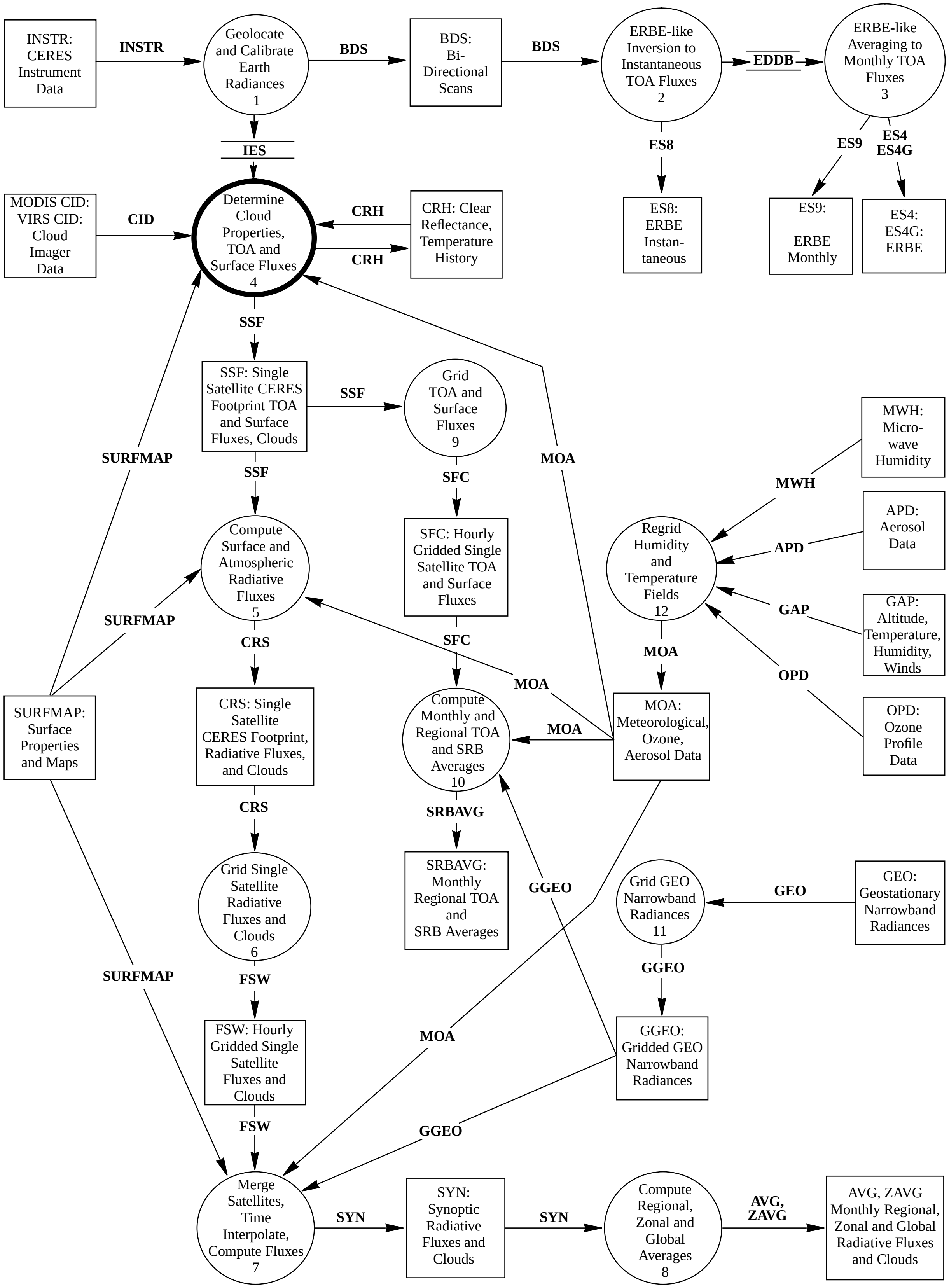

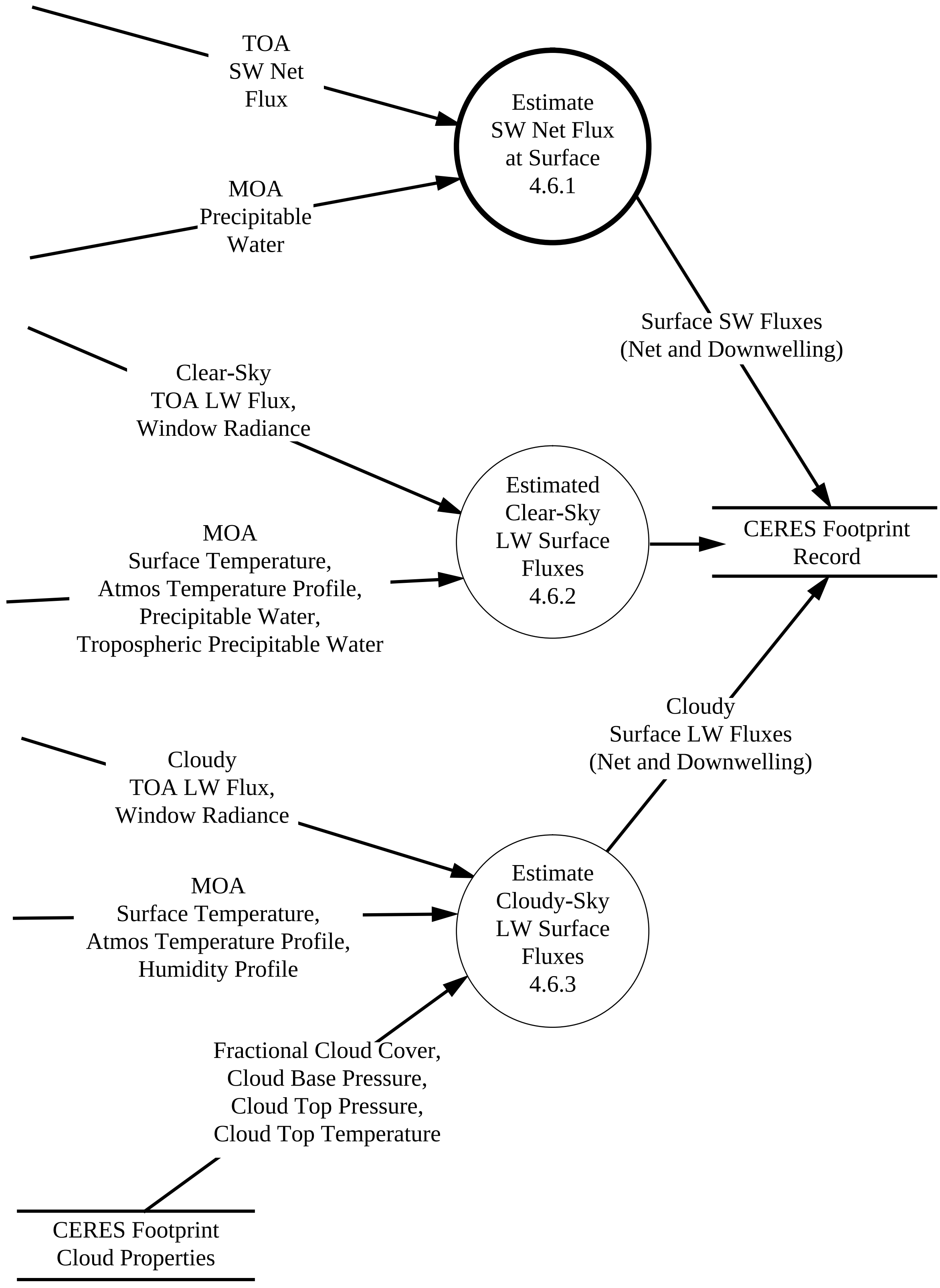

Figure 4.6-1. Major processes for empirical estimation of SW and LW surface radiation budget.

Abstract

A concise review is presented for the algorithm of Li et al. which will be employed to estimate Shortwave Surface Radiation Budget (SW SRB) from CERES measured Top-of-the-Atmosphere (TOA) irradiances. The algorithm is a parameterization scheme resulting from extensive radiative transfer computations. It contains three input parameters: the solar zenith angle, the precipitable water, and the TOA reflected solar flux. The algorithm is applicable to both clear and cloudy conditions for any surface conditions. Its performance has been validated against radiation measurements from towers and conventional radiation network. The accuracy for monthly mean estimates is generally within 10 Wm^{-2} as required for climate studies. Future validation is planned using higher quality and more complete measurements from such programs as the Atmospheric Radiation Measurement (ARM) and Baseline Surface Radiation Network (BSRN), which will overcome some limitations of the previous validation exercises and unravel a controversy concerning the applicability of the algorithm related to cloud absorption.

4.6.1. Estimate of Shortwave Surface Radiation Budget From CERES

4.6.1.1. Introduction

Shortwave surface radiation budget (SW SRB) refers to the net (down minus up) solar radiation absorbed at the Earth's surface over a nominal spectral range 0.2 - 5.0 µm. As the major component of surface heat balance, the importance of SW SRB in Earth's climate is well recognized. A basic requirement for climate studies, especially by virtue of general circulation models (GCMs), is to acquire a climatology of monthly SW SRB with an accuracy of 10 Wm^{-2} on global uniform grids of 250 X 250 km^2 (Suttles and Ohring 1986). While insolation has been observed for over a century, our current knowledge of SW SRB is inferior to that about the Earth's Radiation Budget (ERB) at the TOA which has been monitored from space for only two decades (Li et al. 1996). This seriously hinders climate studies. The major limitations for in-situ SW SRB observation lie in the inability to deploy a uniform observational network of sufficient density, to maintain high operation standards, and to insure proper calibration. Besides, it is very difficult to obtain upwelling flux or albedo representative of large areas from ground-based instruments. Space-borne observation is the only means of providing uniform global measurements.

4.6.1.2. Background

Owing to the intervening atmosphere, SW SRB cannot be measured directly by radiometers aboard spacecraft. Remote sensing techniques are needed to infer SW SRB from the reflected radiance as observed from space. Nevertheless, since the atmosphere emits a negligible amount of radiation in the shortwave region, retrieval of SW SRB is relatively straightforward. Solar energy reaching the Earth is partly reflected to space, partly absorbed in the atmosphere, and partly absorbed at the Earth's surface. Success of retrieving SW SRB thus depends on our ability to account for atmospheric absorption. In contrast to the strong variability of radiation budgets at the TOA and at the surface, atmospheric absorption remains relatively stable; however, the small change in the magnitude of the atmospheric absorption is correlated with the change in the reflected flux at the TOA (Schmetz 1989; Li et al. 1993a). This lays the foundation for estimating SW SRB from TOA satellite measurements.

Ramanathan (1986) noted a simple relationship between the net solar fluxes at the TOA and at the surface by analyzing the results of a GCM. The relationship was explored by Cess and Vulis (1989) with the aid of a more accurate radiative transfer model. They found that variations in TOA and surface net solar fluxes arising from changes in the Solar Zenith Angle (SZA) are correlated in an approximate linear fashion for a given atmospheric and surface condition at small and moderate SZAs. This was corroborated by a comparison between the TOA net fluxes obtained from the Earth Radiation Budget Experiment (ERBE) and the SW SRB data measured from pyranometers mounted on a tower located in Boulder, Colorado (Cess et al. 1991). Based on these matched satellite and surface measurements, Cess et al. (1993) developed an empirical inversion algorithm which worked well under clear skies for a specific location but produced large errors when applied to other conditions. The lack of general applicability originates from the dependence of the relationship on surface albedo, cloud amount, and optical thickness (Li et al. 1993a). While these parameters can be retrieved in principle from satellite measurements, the retrieval is neither easy nor accurate enough. To overcome the limitation, Li et al. (1993a) proposed a new relationship from which a more universal algorithm was formulated.

4.6.1.3. The Algorithm of Li et al.

Instead of relating the net solar fluxes at the TOA and the surface by changing SZA for a fixed atmospheric and surface condition, Li et al. (1993a) established a new relationship between the TOA reflected flux and SW SRB by changing surface albedo and cloud optical thickness for a fixed SZA. By doing so, sensitivities to these factors are eliminated and the new relationship is perfectly linear for all SZAs, as is shown in figure 1. For a given TOA reflected flux and SZA, there is a unique value for SW SRB. Moreover, the relationships for clear and for cloudy conditions exhibit few discrepancies (Li et al., 1993a), implying that SW SRB can be determined reasonably well from a TOA reflected flux without knowledge about surface and sky conditions. Sensitivity tests of the relationship show weak dependence on SZA and water vapor. These effects were taken into account by parameterizing the results of comprehensive radiative transfer calculations for over 100 combinations of different surface, cloud, and atmospheric conditions. The parameterized algorithm is given as below:

$$SW_{\mathrm{surf}}^{\mathrm{net}} = E_o d^{-2}\mu\left\{1 - \frac{C}{\mu} - \frac{D}{\sqrt{\mu}} + \frac{1-\exp(-\mu)}{\mu}(0.0699 - 0.0683\sqrt{p}) - [1 + A + B\,\ln(\mu) - 0.0273 + 0.0216\sqrt{p}]\alpha_{TOA}\right\} \quad (1)$$

where

E_o = solar constant = 1365 W-m^{-2}

d = Earth-Sun distance in astronomical units

p = precipitable water in cm

θ_o = solar zenith angle

$\mu = \cos\theta_o$

α_{TOA} = albedo at TOA = $F_{TOA}/(E_o d^{-2}\mu)$

F_{TOA} = satellite-derived reflected shortwave flux at TOA, W-m^{-2}

A = 0.0815

B = 0.0139

C = –0.01124

D = 0.1487

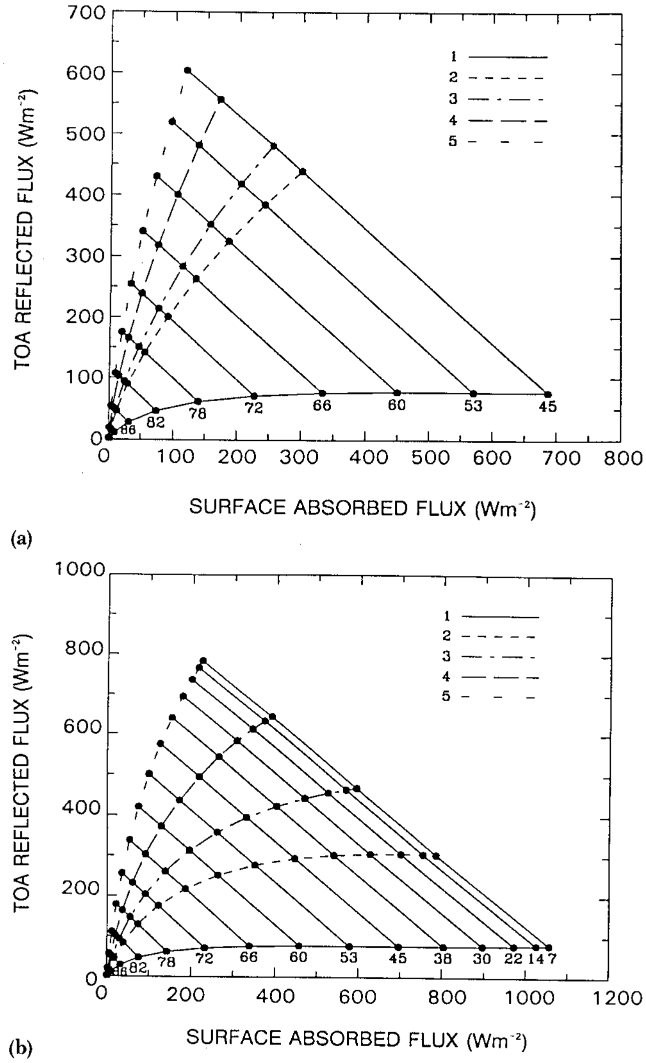

FIG. 1. Relationship between SSRB and reflected flux at the TOA for (a) clear sky, and (b) cloudy sky. Curves 1–5 in (a) represent simulation results for ocean, melting, near melting, aging and fresh snow surfaces under clear sky condition (a), and for cloud optical depths of 0, 5, 10, 20, and 40 for Sc clouds over ocean (b) (Li et al., 1993a).

4.6.1.4 Validation

Two major validation exercises have been conducted. One employs collocated and coincident satellite footprint data of TOA reflected flux and tower measurements of the surface net solar flux (Li et al. 1993b) and another uses monthly mean data obtained from the global surface radiation network and estimated from ERBE using the Li et al. algorithm (Li et al. 1995a). The tower measurements were made over vegetated land in Boulder, Colorado, and snow covered land in Saskatoon, Saskatchewan, Canada (Li et al. 1993b). In addition to distinct surface albedo, the two locations are affected by different cloud regimes. Figure 2 presents the comparisons between observed and estimated SW SRB under both clear- and all-sky conditions. The good agreements confirm that the algorithm is insensitive to surface and sky conditions. The large scatter under cloudy conditions stems from errors incurred in matching the satellite and surface measurements that are prominent when broken cumulus clouds are present (Li et al. 1993b). The match-up error was singled out in a validation of the monthly mean SW SRB product derived from ERBE (Li and Leighton 1993) against surface radiation measurements from the

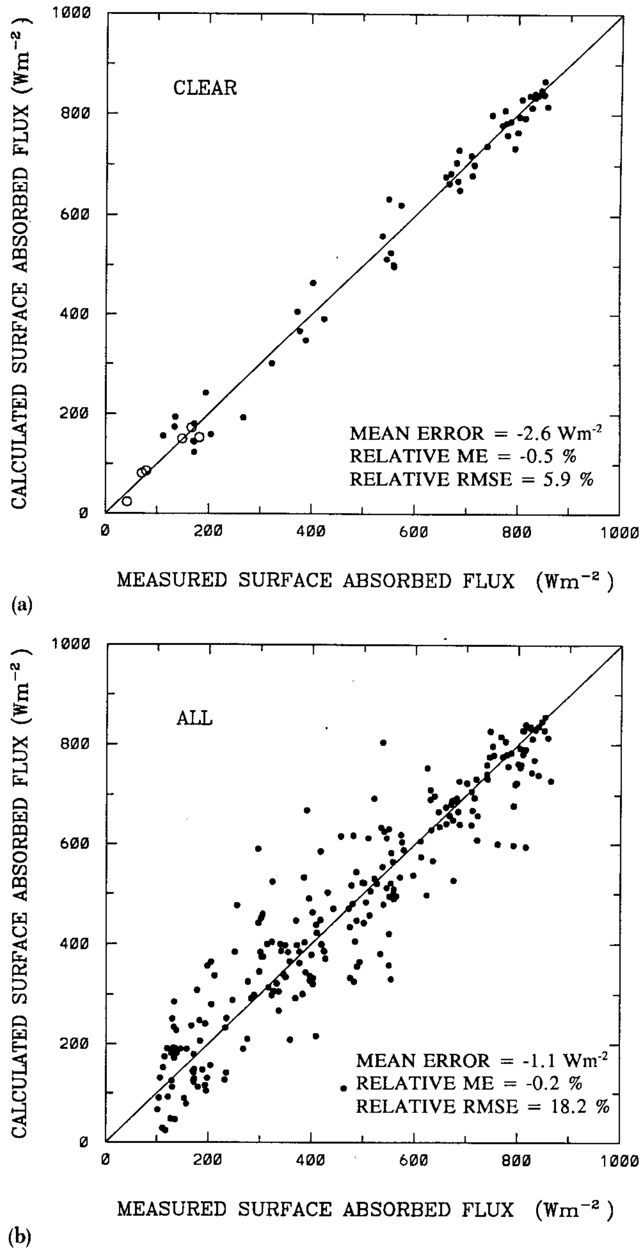

FIG. 2. Comparison between SSRB as estimated from ERBS and as measured at two towers for (a) clear sky, and (b) all sky. For (a) data were available from a tower located in Boulder, Colorado, (solid points) during summer, and a tower in Saskatoon, Saskatchewan, Canada (open points) during winter. All-sky comparison includes the Boulder tower data only (Li et al., 1993b).

Global Energy Balance Archive (GEBA) (Ohmura and Gilgen 1993). As is shown in figure 3, the mean difference remains very small (less than 5 Wm^{-2}), whereas the standard difference (SD) in Wm^{-2} diminishes rapidly with increasing number of surface pyranometers (N) following

$$SD = 4.1 + 24.2 / N \tag{2}$$

SD is composed of a match-up error denoted by the second term (24.2/N) and a true random error of 4.1 Wm^{-2} (Li et al. 1995a). It should be noted that since the areal representation for surface albedo was limited in their studies, Li et al. (1995a) restricted their validation to surface insolation.

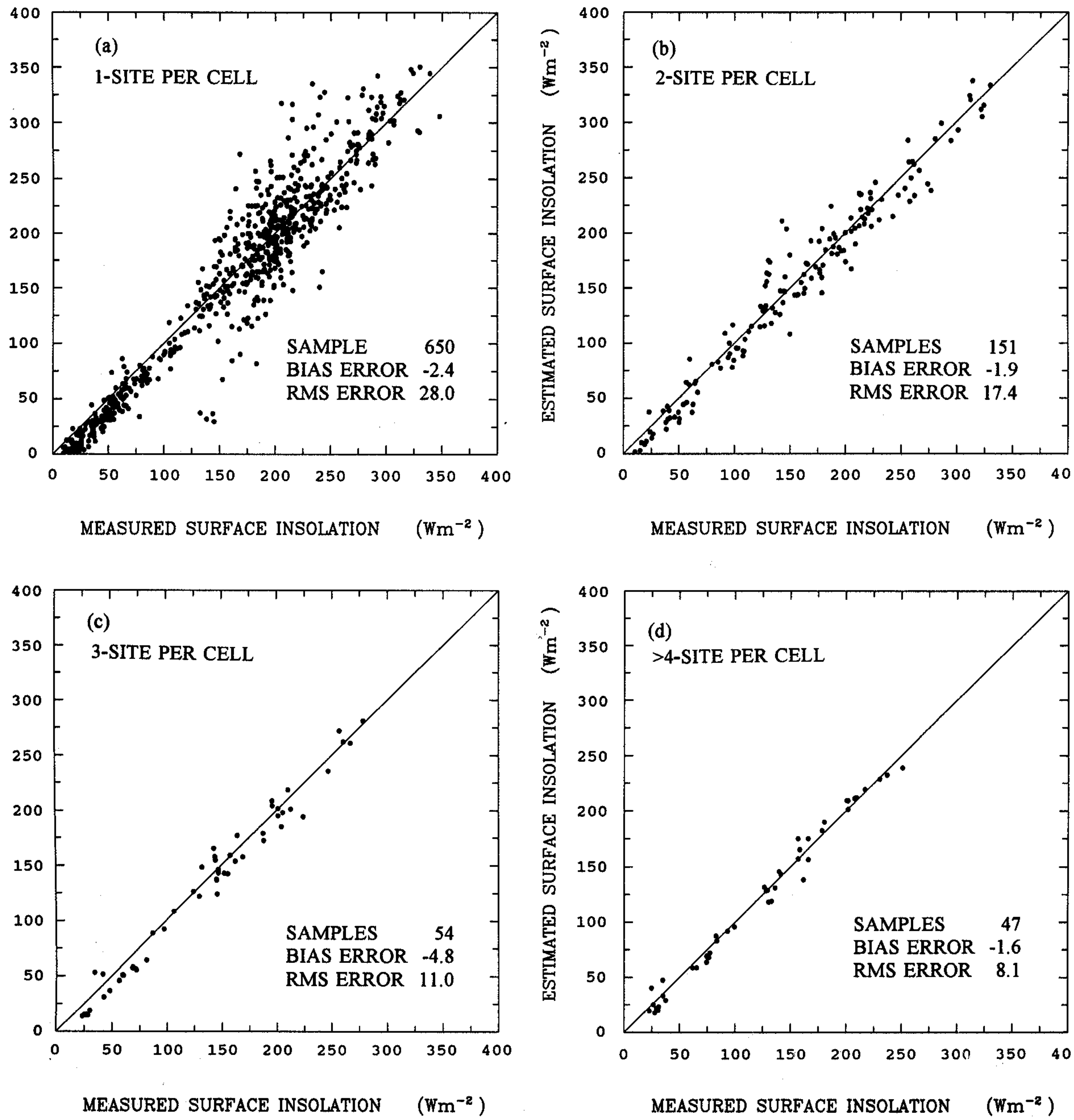

FIG. 3. Comparison of the surface insolation derived from ERBE satellite data with the insolation measured at the surface radiation network from the Global Energy Balance Archive (GEBA) for four categories classified according to the number of surface sites within a cell of 280km * 280km as indicated on the plots (Li et al. 1995a).

While this number is significantly less than the accuracy requirement of 10 Wm^{-2} for climate studies, these validations are insufficient to claim that the requirement is met owing to the following limitations. First, the surface measurements were made from an observation network of highly skewed geographic distribution, mostly in inhabited continental areas. Few data were available over oceans and remote lands including polar regions. Second, considerable match-up errors may have masked estimation uncertainties of similar or smaller magnitudes. Third, lack of information on variables that exert influences on the relationship prevents investigation of their effects. More extensive and meticulous validations are thereby essential to assure and improve the quality of the retrieved SW SRB product. The programs that are of particular value to a further validation include the DOE's Atmospheric Radiation Measurement (ARM) program and the WCRPs Baseline Surface Radiation Network (BSRN). The unique assets of ARM for the validation are the selection of distinct ARM locales representing very different climate and environmental conditions, provision of ample information on radiation sensitive parameters, high density surface radiation networks. While BSRN provides high-quality coherent surface radiation measurements, its utility for the validation exercise is limited by its measurements of point specific nature, and the lack of ancillary data. In addition to providing bulk statistics of the validation results, validation should also include examination of the difference between observed and estimated SW SRB with respect to any factor of potential influence.

4.6.1.5 A Pending Scientific Issue

A doubt has been cast on the validity of the retrieving algorithm following some studies claiming an enormous cloud absorption anomaly (Cess et al. 1995, Ramanathan et al. 1995, Pilewski and Valero, 1995, etc.). These studies suggested that the amount of solar radiation absorbed by clouds is substantially underestimated by the conventional radiative models, indicating that some important physical process may have been overlooked. This finding has, however, been challenged by other studies (Chou et al. 1995, Li et al. 1995b, Arking 1996, etc.). Resolution of this issue may be forthcoming from field programs such as the ARM Enhanced Shortwave Experiment (ARESE). The principal objective of ARESE was to directly measure the absorption of solar radiation for both clear-sky and cloudy-sky conditions and to determine the uncertainties on these measurements. It is hoped that programs such as ARESE will help determine if the claimed cloud absorption anomaly is genuine and, if so, to find the causes of the problem. Until conclusive results are obtained, the most reasonable course of action is to retain the existing algorithm. The results of validation itself may help to prove or disprove the claim. For example, previous validations do not support the finding, as the algorithm performs equally well under clear and cloudy conditions, barring a trade-off between errors due to clouds and due to other factors.

4.6.1.6 Conclusion

This document describes an algorithm for estimating SW SRB from CERES measurements. The algorithm was proposed by Li et al. which consists of a parameterization relating SW SRB to the reflected shortwave flux at the Top-of-the-Atmosphere with the input parameters of the column water vapor amount (precipitable water) and the cosine of the solar zenith angle. The algorithm was derived exclusively from radiative transfer calculations. It has been tested by comparing the net surface flux deduced from broadband radiance measurements from ERBS against surface data from two sets of tower instruments and global surface radiation network. The comparisons showed very small mean difference and moderate standard difference. The latter is associated principally with poor representation of surface observations within a satellite grid-cell. For the monthly mean estimates of SW SRB, the true random error is estimated to be well within 10 Wm^{-2}. Given the ongoing debate regarding cloud absorption, more extensive validation is required. Limitations and future improvements of the algorithm are also addressed.

4.6.1.7 References

Arking, A.; Chou, M.-D.; and Ridgway, W.L. 1996: On Estimating the Effects of Clouds on Atmospheric Absorption Based on Flux Observations Above and Below Cloud Level. *Geophy. Res. Let.*, vol. 23, pp. 829-832.

Cess, R.D; and I.L. Vulis 1989: Inferring Surface Solar Absorption From Broadband Satellite Measurements. *J. Climat*., vol. 2, pp. 974-985.

Cess, Robert D.; Dutton, Ellsworth G.; Deluisi, John J.; and Jiang, Feng 1991: Determining Surface Solar Absorption From Broadband Satellite Measurements for Clear Skies—Comparison With Surface Measurements. *J. Climat*., vol. 4, pp. 236–247.

Cess, R.D.; Nemesure, S.; Dutton, E.G.; DeLuisi, J.J.; Potter,G.L.; and Morcrette, J.-J. 1993: The Impact of Clouds on the Shortwave Radiation Budget of the Surface-Atmosphere System: Interfacing Measurements and Model. *J. Climat*., vol. 6, pp. 308-316.

Cess, R. D.; Zhang, M. H.; Minnis, P.; Corsetti, L.; Dutton, E. G.; Forgan, B. W.; Garber, D. P.; Gates, W. L.; Hack, J. J.; Harrison, E. F.; Jing, X.; Kiehl, J. T.; Long, C. N.; Morcrette, J.-J.; Potter, G. L.; Ramanathan, V.; Subasilar, B.; Whitlock, C. H.; Young, D. F.; and Zhou, Y. 1995: Absorption of Solar Radiation by Clouds: Observations Versus Models. *Science*, vol. 267, pp. 496–499.

Chou, M.-D.; Arking, A.; Otterman, J.; and Ridgway, W. L. 1995: The Effects of Clouds on Atmospheric Absorption of Solar Radiation. *Geophy. Res. Let.*, vol. 22, pp. 1885-1888.

Li, Zhanqing; Leighton, H. G.; Masuda, Kazuhiko; and Takashima, Tsutomu 1993a: Estimation of SW Flux Absorbed at the Surface From TOA Reflected Flux. *J. Climat.*, vol. 6, no. 2, pp. 317–330.

Li, Zhanqing; Leighton, H. G.; and Cess, Robert D. 1993b: Surface Net Solar Radiation Estimated From Satellite Measurements—Comparisons With Tower Observations. *J. Climat.*, vol. 6, no. 9, pp. 1764–1772.

Li, Z.; and Leighton, H.G. 1993: Global Climatologies of Solar Radiation Budgets at the Surface and in the Atmosphere From 5 Years of ERBE Data. *J. Geophy. Res.*, vol. 98, pp. 4919-4930.

Li, Z.; Whitlock, C. H.; and Charlock, T. P. 1995a: Assessment of the Global Monthly Mean Surface Insolation Estimated From Satellite Measurements Using Global Energy Balance Archive Data. *J. Climat.*, vol. 8, pp. pp. 315-*328.*

Li, Z.; Barker, H. W.; and Moreau, L. 1995b: The Variable Effect of Clouds on Atmospheric Absorption of Solar Radiation. *Nature,* vol. 376, pp. 486–490.

Li, Z.; Moreau, L.; and Arking, A. 1996: On Solar Energy Disposition, A Perspective From Observation and Modeling. *Bull. Amer. Meteor. Soc.*, in press.

Pilewski, P.; and Valero, F. P. J. 1995: Direct Observations of Excess Solar Absorption by Clouds. *Science*, vol. 267, pp. 1626–1629.

Ohmura, A.; and Gilgen, H. 1993: Re-evaluation of the Global Energy Balance. Geophy. Monogra. 75, *American Geophy. Union*, vol. 15, pp. 93-110.

Ramanathan, V. 1986: Scientific Use of Surface Radiation Budget for Climate Studies. Report of the Workshop on Surface Radiation Budget for Climate Applications. NASA RP-1169, pp. 58-86.

Ramanathan, V.; Subasilar, B.; Zhang, G. J.; Conant, W.; Cess, R. D.; Kiehl, J. T.; Grassl, H.; and Shi, L. 1995: Warm Pool Heat Budget and Shortwave Cloud Forcing: A Missing Physics? *Science,* vol. 267, pp. 499–503.

Schmetz, J. 1989: Towards a Surface Radiation Climatology: Retrieval of Downward Irradiance From Satellite. *Atmos. Res.*, vol. 23, pp. 287-321.

Suttles, J.T.; and Ohring, G. 1986: Surface Radiation Budget for Climate Applications. NASA Reference Publication 1169, 132 pp.

Appendix A

Nomenclature

Acronyms

ADEOS	Advanced Earth Observing System
ADM	Angular Distribution Model
AIRS	Atmospheric Infrared Sounder (EOS-AM)
AMSU	Advanced Microwave Sounding Unit (EOS-PM)
APD	Aerosol Profile Data
APID	Application Identifier
ARESE	ARM Enhanced Shortwave Experiment
ARM	Atmospheric Radiation Measurement
ASOS	Automated Surface Observing Sites
ASTER	Advanced Spaceborne Thermal Emission and Reflection Radiometer
ASTEX	Atlantic Stratocumulus Transition Experiment
ASTR	Atmospheric Structures
ATBD	Algorithm Theoretical Basis Document
AVG	Monthly Regional, Average Radiative Fluxes and Clouds (CERES Archival Data Product)
AVHRR	Advanced Very High Resolution Radiometer
BDS	Bidirectional Scan (CERES Archival Data Product)
BRIE	Best Regional Integral Estimate
BSRN	Baseline Surface Radiation Network
BTD	Brightness Temperature Difference(s)
CCD	Charge Coupled Device
CCSDS	Consultative Committee for Space Data Systems
CEPEX	Central Equatorial Pacific Experiment
CERES	Clouds and the Earth’s Radiant Energy System
CID	Cloud Imager Data
CLAVR	Clouds from AVHRR
CLS	Constrained Least Squares
COPRS	Cloud Optical Property Retrieval System
CPR	Cloud Profiling Radar
CRH	Clear Reflectance, Temperature History (CERES Archival Data Product)
CRS	Single Satellite CERES Footprint, Radiative Fluxes and Clouds (CERES Archival Data Product)
DAAC	Distributed Active Archive Center
DAC	Digital-Analog Converter
DAO	Data Assimilation Office

DB	Database
DFD	Data Flow Diagram
DLF	Downward Longwave Flux
DMSP	Defense Meteorological Satellite Program
EADM	ERBE-Like Albedo Directional Model (CERES Input Data Product)
ECA	Earth Central Angle
ECLIPS	Experimental Cloud Lidar Pilot Study
ECMWF	European Centre for Medium-Range Weather Forecasts
EDDB	ERBE-Like Daily Data Base (CERES Archival Data Product)
EID9	ERBE-Like Internal Data Product 9 (CERES Internal Data Product)
EOS	Earth Observing System
EOSDIS	Earth Observing System Data Information System
EOS-AM	EOS Morning Crossing Mission
EOS-PM	EOS Afternoon Crossing Mission
ENSO	El Niño/Southern Oscillation
ENVISAT	Environmental Satellite
EPHANC	Ephemeris and Ancillary (CERES Input Data Product)
ERB	Earth Radiation Budget
ERBE	Earth Radiation Budget Experiment
ERBS	Earth Radiation Budget Satellite
ESA	European Space Agency
ES4	ERBE-Like S4 Data Product (CERES Archival Data Product)
ES4G	ERBE-Like S4G Data Product (CERES Archival Data Product)
ES8	ERBE-Like S8 Data Product (CERES Archival Data Product)
ES9	ERBE-Like S9 Data Product (CERES Archival Data Product)
FLOP	Floating Point Operation
FIRE	First ISCCP Regional Experiment
FIRE II IFO	First ISCCP Regional Experiment II Intensive Field Observations
FOV	Field of View
FSW	Hourly Gridded Single Satellite Fluxes and Clouds (CERES Archival Data Product)
FTM	Functional Test Model
GAC	Global Area Coverage (AVHRR data mode)
GAP	Gridded Atmospheric Product (CERES Input Data Product)
GCIP	GEWEX Continental-Phase International Project
GCM	General Circulation Model
GEBA	Global Energy Balance Archive
GEO	ISSCP Radiances (CERES Input Data Product)
GEWEX	Global Energy and Water Cycle Experiment

GLAS	Geoscience Laser Altimetry System
GMS	Geostationary Meteorological Satellite
GOES	Geostationary Operational Environmental Satellite
HBTM	Hybrid Bispectral Threshold Method
HIRS	High-Resolution Infrared Radiation Sounder
HIS	High-Resolution Interferometer Sounder
ICM	Internal Calibration Module
ICRCCM	Intercomparison of Radiation Codes in Climate Models
ID	Identification
IEEE	Institute of Electrical and Electronics Engineers
IES	Instrument Earth Scans (CERES Internal Data Product)
IFO	Intensive Field Observation
INSAT	Indian Satellite
IOP	Intensive Observing Period
IR	Infrared
IRIS	Infrared Interferometer Spectrometer
ISCCP	International Satellite Cloud Climatology Project
ISS	Integrated Sounding System
IWP	Ice Water Path
LAC	Local Area Coverage (AVHRR data mode)
LaRC	Langley Research Center
LBC	Laser Beam Ceilometer
LBTM	Layer Bispectral Threshold Method
Lidar	Light Detection and Ranging
LITE	Lidar In-Space Technology Experiment
Lowtran 7	Low-Resolution Transmittance (Radiative Transfer Code)
LW	Longwave
LWP	Liquid Water Path
MAM	Mirror Attenuator Mosaic
MC	Mostly Cloudy
MCR	Microwave Cloud Radiometer
METEOSAT	Meteorological Operational Satellite (European)
METSAT	Meteorological Satellite
MFLOP	Million FLOP
MIMR	Multifrequency Imaging Microwave Radiometer
MISR	Multiangle Imaging Spectroradiometer
MLE	Maximum Likelihood Estimate
MOA	Meteorology Ozone and Aerosol
MODIS	Moderate-Resolution Imaging Spectroradiometer

MSMR	Multispectral, multiresolution
MTSA	Monthly Time and Space Averaging
MWH	Microwave Humidity
MWP	Microwave Water Path
NASA	National Aeronautics and Space Administration
NCAR	National Center for Atmospheric Research
NCEP	National Centers for Environmental Prediction
NESDIS	National Environmental Satellite, Data, and Information Service
NIR	Near Infrared
NMC	National Meteorological Center
NOAA	National Oceanic and Atmospheric Administration
NWP	Numerical Weather Prediction
OLR	Outgoing Longwave Radiation
OPD	Ozone Profile Data (CERES Input Data Product)
OV	Overcast
PC	Partly Cloudy
POLDER	Polarization of Directionality of Earth’s Reflectances
PRT	Platinum Resistance Thermometer
PSF	Point Spread Function
PW	Precipitable Water
RAPS	Rotating Azimuth Plane Scan
RPM	Radiance Pairs Method
RTM	Radiometer Test Model
SAB	Sorting by Angular Bins
SAGE	Stratospheric Aerosol and Gas Experiment
SARB	Surface and Atmospheric Radiation Budget Working Group
SDCD	Solar Distance Correction and Declination
SFC	Hourly Gridded Single Satellite TOA and Surface Fluxes (CERES Archival Data Product)
SHEBA	Surface Heat Budget in the Arctic
SPECTRE	Spectral Radiance Experiment
SRB	Surface Radiation Budget
SRBAVG	Surface Radiation Budget Average (CERES Archival Data Product)
SSF	Single Satellite CERES Footprint TOA and Surface Fluxes, Clouds
SSMI	Special Sensor Microwave Imager
SST	Sea Surface Temperature
SURFMAP	Surface Properties and Maps (CERES Input Product)
SW	Shortwave
SWICS	Shortwave Internal Calibration Source

SYN	Synoptic Radiative Fluxes and Clouds (CERES Archival Data Product)
SZA	Solar Zenith Angle
THIR	Temperature/Humidity Infrared Radiometer (Nimbus)
TIROS	Television Infrared Observation Satellite
TISA	Time Interpolation and Spatial Averaging Working Group
TMI	TRMM Microwave Imager
TOA	Top of the Atmosphere
TOGA	Tropical Ocean Global Atmosphere
TOMS	Total Ozone Mapping Spectrometer
TOVS	TIROS Operational Vertical Sounder
TRMM	Tropical Rainfall Measuring Mission
TSA	Time-Space Averaging
UAV	Unmanned Aerospace Vehicle
UT	Universal Time
UTC	Universal Time Code
VAS	VISSR Atmospheric Sounder (GOES)
VIRS	Visible Infrared Scanner
VISSR	Visible and Infrared Spin Scan Radiometer
WCRP	World Climate Research Program
WG	Working Group
Win	Window
WN	Window
WMO	World Meteorological Organization
ZAVG	Monthly Zonal and Global Average Radiative Fluxes and Clouds (CERES Archival Data Product)

Symbols

A	atmospheric absorptance
$B_\lambda(T)$	Planck function
C	cloud fractional area coverage
CF_2Cl_2	dichlorofluorocarbon
$CFCl_3$	trichlorofluorocarbon
CH_4	methane
CO_2	carbon dioxide
D	total number of days in the month
D_e	cloud particle equivalent diameter (for ice clouds)
E_o	solar constant or solar irradiance
F	flux
f	fraction

G_a	atmospheric greenhouse effect
g	cloud asymmetry parameter
H_2O	water vapor
I	radiance
i	scene type
m_i	imaginary refractive index
$\hat{N}$	angular momentum vector
N_2O	nitrous oxide
O_3	ozone
P	point spread function
p	pressure
Q_a	absorption efficiency
Q_e	extinction efficiency
Q_s	scattering efficiency
R	anisotropic reflectance factor
r_E	radius of the Earth
r_e	effective cloud droplet radius (for water clouds)
r_h	column-averaged relative humidity
S_o	summed solar incident SW flux
S_o'	integrated solar incident SW flux
T	temperature
T_B	blackbody temperature
t	time or transmittance
W_{liq}	liquid water path
w	precipitable water
$\hat{x}_o$	satellite position at t_o
x, y, z	satellite position vector components
$\dot{x}, \dot{y}, \dot{z}$	satellite velocity vector components
z	altitude
z_{top}	altitude at top of atmosphere
α	albedo or cone angle
β	cross-scan angle
γ	Earth central angle
γ_{at}	along-track angle
γ_{ct}	cross-track angle
δ	along-scan angle
ε	emittance
Θ	colatitude of satellite
θ	viewing zenith angle

θ_o	solar zenith angle
λ	wavelength
μ	viewing zenith angle cosine
μ_o	solar zenith angle cosine
ν	wave number
ρ	bidirectional reflectance
τ	optical depth
$\tau_{aer}(p)$	spectral optical depth profiles of aerosols
$\tau_{H_2O\lambda}(p)$	spectral optical depth profiles of water vapor
$\tau_{O_3}(p)$	spectral optical depth profiles of ozone
Φ	longitude of satellite
ϕ	azimuth angle
$\tilde{\omega}_o$	single-scattering albedo

Subscripts:

c	cloud
cb	cloud base
ce	cloud effective
cld	cloud
cs	clear sky
ct	cloud top
ice	ice water
lc	lower cloud
liq	liquid water
s	surface
uc	upper cloud
λ	spectral wavelength

Units

AU	astronomical unit
cm	centimeter
cm-sec^{-1}	centimeter per second
count	count
day	day, Julian date
deg	degree
deg-sec^{-1}	degree per second
DU	Dobson unit
erg-sec^{-1}	erg per second
fraction	fraction (range of 0–1)
g	gram

$g\text{-}cm^{-2}$	gram per square centimeter
$g\text{-}g^{-1}$	gram per gram
$g\text{-}m^{-2}$	gram per square meter
h	hour
hPa	hectopascal
K	Kelvin
kg	kilogram
$kg\text{-}m^{-2}$	kilogram per square meter
km	kilometer
$km\text{-}sec^{-1}$	kilometer per second
m	meter
mm	millimeter
μm	micrometer, micron
N/A	not applicable, none, unitless, dimensionless
$ohm\text{-}cm^{-1}$	ohm per centimeter
percent	percent (range of 0–100)
rad	radian
$rad\text{-}sec^{-1}$	radian per second
sec	second
sr^{-1}	per steradian
W	watt
$W\text{-}m^{-2}$	watt per square meter
$W\text{-}m^{-2}sr^{-1}$	watt per square meter per steradian
$W\text{-}m^{-2}sr^{-1}\mu m^{-1}$	watt per square meter per steradian per micrometer